

**CONFIDENTIAL**Copy 5  
RM L52A24

NACA RM L52A24

FOR INFORMATION MAR 27 1952

**RESEARCH MEMORANDUM**

EXPERIMENTAL INVESTIGATION OF INTERNAL-FLOW  
 CHARACTERISTICS OF FORWARD UNDERSLUNG  
 FUSELAGE SCOOPS WITH UNSWEPT AND  
 SWEPTBACK ENTRANCES AT MACH  
 NUMBERS OF 1.41 TO 1.96

By Robert W. Boswinkle, Jr. and Meade H. Mitchell, Jr.

Langley Aeronautical Laboratory  
 Langley Field, Va.

CLASSIFICATION CANCELLED

Att. by NACA Res. 684 Date 4/11/56

RN 96

By NACA 2/17/56 See

CLASSIFIED DOCUMENT

This material contains information affecting the National Defense of the United States within the meaning of the espionage laws, Title 18, U.S.C., Secs. 793 and 794, the transmission or revelation of which in any manner to unauthorized person is prohibited by law.

**NATIONAL ADVISORY COMMITTEE  
 FOR AERONAUTICS**

WASHINGTON  
 March 6, 1952

**CONFIDENTIAL**

NACA LIBRARY  
 LANGLEY AERONAUTICAL LABORATORY  
 Langley Field, Va.

## NATIONAL ADVISORY COMMITTEE FOR AERONAUTICS

## RESEARCH MEMORANDUM

## EXPERIMENTAL INVESTIGATION OF INTERNAL-FLOW

## CHARACTERISTICS OF FORWARD UNDERSLUNG

## FUSELAGE SCOOPS WITH UNSWEPT AND

## SWEPTBACK ENTRANCES AT MACH


## NUMBERS OF 1.41 TO 1.96

By Robert W. Boswinkle, Jr. and Meade H. Mitchell, Jr.

## SUMMARY

Two versions of a type of forward underslung scoop mounted on a pointed fuselage were investigated, principally at a Mach number of 1.41, in the Langley 9- by 12-inch supersonic blowdown tunnel. The scoop entrances were in the shape of a  $60^\circ$  sector of an annulus; the sides of one scoop were unswept and the sides of the other were sweptback. Total-pressure recoveries, surface-pressure distributions, and shadowgraphs were obtained over wide ranges of angle of attack and mass-flow ratio. A few tests at Mach numbers of 1.62 and 1.96 were also made.

At a Mach number of 1.41, a mass-flow ratio of 0.95, and zero angle of attack each scoop provided a total-pressure recovery approximately equal to that across a normal shock at the free-stream Mach number; as the mass-flow ratio was decreased the total-pressure recovery of the unswept scoop remained nearly constant whereas that of the sweptback scoop decreased appreciably. The total-pressure recoveries of both scoops were higher at an angle of attack of  $10^\circ$  than at  $0^\circ$  throughout the mass-flow-ratio range. Although drag measurements at transonic and low supersonic speeds as well as additional total-pressure recovery measurements at transonic speeds are needed to evaluate finally the worth of the scoop designs, the unswept scoop appears to be a satisfactory configuration from a total-pressure-recovery standpoint at a Mach number of 1.41.



## INTRODUCTION

A scoop-type air inlet is often prescribed for an aircraft design primarily because the front part of the fuselage, where a nose inlet alternatively might be placed, is needed for radar, armament, and other equipment. Efficient supersonic scoops (such as that of reference 1) usually incorporate boundary-layer-control devices and means for obtaining efficient supersonic compression of the entering flow. The scoop (such as that of reference 2) located well forward on the expanding part of a pointed fuselage is a special case: The short length of boundary-layer run with a favorable pressure gradient over most of the length may render boundary-layer control unnecessary, and the oblique shock from the fuselage nose may provide adequate supersonic compression for low supersonic Mach numbers (values below 1.5). Also, when interference effects on the fuselage are neglected, a scoop located in the reduced-velocity region behind the nose shock would be expected to have lower drag than a scoop located farther rearward.

Because the forward underslung scoop for the low-supersonic-speed airplane seemed promising, an experimental investigation was undertaken to study, principally at a Mach number of 1.41, the internal-flow characteristics of an unswept and a sweptback version of this type of inlet. For both scoop models the entrance shape chosen was a 60° sector of an annulus; this shape provided a large capture area within the frontal area of the basic fuselage and at the same time had features, a small width and orthogonal corners at the fuselage surface, which were thought to be favorable from a total-pressure-recovery standpoint. No attempt was made to develop an optimum lip shape or to measure the drag because of the preliminary nature of the investigation.

Presented herein are total-pressure recoveries, surface-pressure distributions, and shadowgraphs obtained for each scoop at a Mach number of 1.41 over wide ranges of mass-flow ratio and angle of attack. The results of a few tests at Mach numbers of 1.62 and 1.96 are also presented although it is not expected that these particular scoop configurations will be used at Mach numbers in this range.

## SYMBOLS

$\bar{H}/H_0$	ratio of average total pressure (average weighted according to mass flow) at duct exit to free-stream total pressure
$m/m_0$	ratio of mass flow entering scoop to mass flow in a free-stream tube of same cross-sectional area as entrance throat area of scoop

$M_0$	free-stream Mach number
$p/H_0$	ratio of static pressure on fuselage surface to free-stream total pressure
$\alpha$	angle of attack, degrees

#### APPARATUS AND TESTS

The model was built to simulate the forward part of the fuselage and the scoop of a possible low-supersonic-speed airplane (fig. 1). Since, for the tests reported herein, drag measurements were not made, no attempt was made to simulate an airplane configuration rearward of the inlet. Photographs and drawings of the model are presented as figures 2 and 3, respectively.

Each scoop had an entrance in the shape of a  $60^\circ$  sector of an annulus, the inner boundary being the fuselage surface and the outer being the outer lip of the scoop; this shape was then modified by rounding the outer corners as shown in figures 3(b) and 3(c). This particular entrance shape was chosen since it provided a sufficiently large capture area within the frontal area of the basic fuselage; presented a small scoop width at the fuselage surface which, together with the forward location of the scoop, should tend to minimize the amount of boundary layer in the entering flow; and resulted in orthogonal corners at the circular fuselage surface which should effect less total-pressure losses in the duct than the acute corners resulting from a parallel-sided scoop.

The lip shape for each scoop consisted of a wedge with a leading-edge radius of 0.01 inch. The entrance throat areas (measured in a plane just inside the inlet normal to an assumed average direction of the flow) of the two scoops were the same, 0.871 square inch. The shape of the duct cross sections for each scoop was varied downstream of the entrance to form, eventually, a rectangular section with rounded outer corners. The cross-sectional area increased continually from the inlet throat to the maximum area. The exit blocks formed a contracting section at the exit of the duct.

The sides of the unswept scoop were in a plane normal to the model center line. The maximum area in the duct was 1.46 times the inlet area.

The sides of the sweptback scoop were swept  $45^\circ$  with respect to a plane normal to the model center line. The beginning of the sweptback scoop was at the same station as the plane of the inlet for the unswept scoop. The maximum area in the duct for the sweptback scoop was 1.33 times the inlet area.

The fuselage was constructed of laminations of aluminum alloy and wood. The ducts were formed from laminations of fiber glass sheets, the sheets being bonded together with a plastic. Various removable blocks, such as the surface fairings and exit blocks, were made from a plastic.

The model was mounted on its side in the tunnel. The angle of attack was changed by pivoting the model about the pivot bolt shown in figure 3(a) and placing a second bolt through the forward hole in the fuselage corresponding to the desired angle of attack. The mass flow was varied by changing the exit area of the duct by means of several interchangeable exit blocks. Two rakes of three tubes each (as shown in fig. 3(a)) were installed at the exit to measure the total-pressure recovery. A static orifice was installed in each exit block in the plane of the total-pressure tubes which, when uniform static pressure across the duct cross section was assumed, allowed the mass flow also to be measured at the exit. Orifices (shown in fig. 2(b)) in the fuselage surface provided means for obtaining surface-pressure distributions on the fuselage from in front of the inlet to inside the duct.

The Langley 9- by 12-inch supersonic blowdown tunnel, in which the tests were made, uses the compressed air of the Langley 19-foot pressure tunnel. The entering air, which is dried and heated to minimize condensation effects, has an absolute stagnation pressure which ranges from 2 to  $2\frac{1}{3}$  atmospheres. Additional information concerning the tunnel is contained in reference 3.

The average Reynolds numbers per inch at the test Mach numbers of 1.41, 1.62, and 1.96 were  $0.69 \times 10^6$ ,  $0.64 \times 10^6$ , and  $0.56 \times 10^6$ , respectively. Data were obtained for angles of attack from  $-5^\circ$  to  $15^\circ$  and for a range of mass-flow ratio which extended to values above unity.

Pressures were recorded by photographing a multitube mercury manometer. The accuracy of the data presented herein is estimated to be within the following limits:  $p/H_0$  and  $H/H_0$ ,  $\pm 0.008$ ;  $m/m_0$  at  $\frac{m}{m_0} = 0.60$ ,  $\pm 0.06$ ; and  $m/m_0$  at  $\frac{m}{m_0} = 1.00$ ,  $\pm 0.03$ .

## RESULTS AND DISCUSSION

### Shadowgraphs and Surface-Pressure Distributions

Shadowgraphs of the flow about the unswept scoop and the sweptback scoop are shown in figure 4. The shadowgraphs are arranged with constant

values of angle of attack in vertical rows and nearly constant values of mass-flow ratio in horizontal rows. The horizontal lines in some of the shadowgraphs are reference wires placed on one window outside the tunnel.

No-flow shadowgraphs are shown in figure 5. Note that the lines which show up in the no-flow shadowgraphs because of the optical imperfections in the glass windows happen to be oriented so as to obscure somewhat the recognition of Mach lines from the lower part of the model in the flow shadowgraphs.

Surface-pressure distributions are presented in figure 6 for the unswept scoop and in figure 7 for the sweptback scoop; figures 6(a) and 7(a) show the locations of the surface orifices. In this section all discussion is for  $M_0 = 1.41$ .

In general, the shadowgraphs and surface-pressure distributions for both scoops show that, as would be expected, increases in mass-flow ratio move the scoop shock (strong shock in front of inlet) downstream toward the inlet and increases in angle of attack move the scoop shock upstream.

Unswept scoop.- It may be well to point out the various shocks in one of the shadowgraphs of the unswept scoop; for this purpose observe the shadowgraph in figure 4(a) for  $\alpha = 10^\circ$ ,  $\frac{m}{m_0} = 0.39$ . On the left side a short length of the nearly straight oblique shock from the nose is visible. The oblique nose shock joins the scoop shock which stands well in front of the inlet. For this low mass-flow ratio a large quantity of air is spilling around the lower lip. An expansion of this flow occurs and is followed by a compression shock just rearward of the lip. The expansion somewhat distorts the appearance of the lip in the shadowgraphs. For the higher mass-flow ratios and angles of attack, less flow spills around the lip and the shock disappears. What appears to be an additional shock farther downstream from the lip is actually the intersection of the scoop shock with the tunnel windows.

In some of the shadowgraphs (fig. 4(a)) a very weak shock caused by an imperfect juncture at station 2.30 (see fig. 3(a)) between the surface fairing insert and the fuselage is visible (for example, the shadowgraph for  $\alpha = 5^\circ$ ,  $\frac{m}{m_0} = 1.08$ ). Although, in some cases, this shock appears to alter slightly the shape of the scoop shock, the effects of this weak shock are not believed to affect seriously the total-pressure-recovery data beyond the fact that the boundary layer downstream of station 2.30 was probably made turbulent.

Well-defined scoop shocks are indicated (fig. 4(a)) in all the side-view shadowgraphs except for the conditions  $\alpha = -5^\circ$ ,  $\frac{m}{m_0} = 0.73$ ;  $0^\circ$ ,

0.58; and  $0^\circ$ , 0.74. For these conditions no well-defined shocks nor rises in the pressure distributions of figure 6 are shown for the region in front of the entrance. This result may be caused by flow separation in front of the entrance, or by a rapid shock oscillation which was not stopped by the  $\frac{1}{60}$ -second shutter speed of the shadowgraph camera nor observed as fluctuations in the manometer liquid. Although this phenomenon is not completely understood, these mass-flow ratios at  $M_0 = 1.41$  are probably not in the range of much interest.

Sweptback scoop.- The side-view shadowgraphs of the sweptback scoop are shown in figure 4(d). It should be mentioned again that the beginning of the sweptback scoop was at the same station as the plane of the inlet for the unswept scoop. A further guide to establishing a corresponding station on the fuselage for the two scoops is furnished by the weak shock at station 2.30 (discussed in the preceding section).

In the side-view shadowgraphs of the sweptback scoop (fig. 4(d)) for  $\alpha = -5^\circ$ ,  $\frac{m}{m_0} = 0.92$  a weak oblique shock is visible just in front of the scoop entrance. This weak oblique shock appears to originate at the intersection of the scoop sides with the fuselage surface. The scoop shock is located farther downstream. Practically all the supersonic compression occurs through the scoop shock as evidenced by the surface-pressure distributions of figure 7(b). In the other shadowgraphs of figure 4(d) the weak oblique shock remains fixed in position as the strong shock moves forward with decreases in mass-flow ratio and increases in angle of attack. For  $\alpha = 0^\circ$ ,  $\frac{m}{m_0} = 0.58$  and 0.75 the scoop shock coincides with the weak oblique shock and the combined shock has a large inclination to the surface.

#### Total-Pressure Recovery

The average total-pressure recovery measured at the exits of the ducts of the unswept and sweptback scoops are shown as functions of mass-flow ratio in figure 8 for  $M_0 = 1.41$ .

At  $\alpha = 0^\circ$  (fig. 8(b)), for a possible design mass-flow ratio of 0.95, the total-pressure recovery for both scoops is about equal to that across a normal shock at a Mach number of 1.41; as the mass-flow ratio is decreased the total-pressure recovery of the unswept scoop remains nearly constant whereas that of the sweptback scoop decreases appreciably. These diverse total-pressure-recovery characteristics for the two scoops are believed to be caused in large measure by boundary-layer differences at the entrances. This belief stems from the following considerations. At  $\alpha = 0^\circ$  for both scoops the fuselage boundary layer

would be expected to flow in nearly an axially symmetrical manner up to the region of pressure rise caused by the scoop shock. In the case of the sweptback scoop, where the principal part of the compression occurs within or at the beginning of the sweptback sides, the boundary layer has little choice other than to flow directly into the inlet. Since the thickness of the boundary layer increases with decreases in mass-flow ratio, a notable decrease in total-pressure recovery occurs. In the case of the unswept scoop, however, as the mass-flow ratio is decreased the forward movement of the scoop shock makes available a greater length ahead of the inlet for the thickened boundary layer to sweep around the sides of the scoop.

At  $\alpha = 10^\circ$  (fig. 8(d)) the total-pressure recoveries for both scoops are higher than at  $0^\circ$  throughout the mass-flow-ratio range with the greater increase occurring for the sweptback scoop; also, in contrast to the behavior at  $\alpha = 0^\circ$ , the total-pressure recovery for the sweptback scoop varies only a small amount over a wide range of mass-flow ratio. An increase in total-pressure recovery from  $\alpha = 0^\circ$  to  $10^\circ$  would be expected on the basis of the decreased Mach number (which reduces the total-pressure loss through any shocks) at  $\alpha = 10^\circ$  on the underside of the fuselage; calculations have shown, however, that this effect does not account for the principal part of the increase for the unswept scoop at low mass-flow ratios or for the sweptback scoop at any mass-flow ratio. A significant factor in the increase of total-pressure recovery from  $\alpha = 0^\circ$  to  $10^\circ$  is believed to be a cross flow of the boundary layer around the fuselage at an angle of attack; boundary-layer cross flow around a body at an angle of attack has been observed frequently in other investigations. The cross flow may occur even upstream of the scoop shock so that, even for the sweptback scoop, less boundary layer enters the inlet; the result is that high total-pressure recovery is maintained for both scoops over a wide range of mass-flow ratio at  $\alpha = 10^\circ$ .

The average total-pressure ratios as functions of mass-flow ratio are shown in figures 9 and 10 for Mach numbers of 1.62 and 1.96. In these figures the total-pressure recovery is generally higher for the unswept scoop and the values fall off less rapidly with decreases in mass-flow ratio than for the sweptback scoop. The superiority of the unswept scoop over the sweptback scoop at low mass-flow ratios and zero angle of attack at these higher Mach numbers is believed again to be caused partially by the greater ability of the unswept scoop to shed the boundary layer around the sides of the scoop.

Cross plots of figures 8 to 10 given as figure 11 show the variation of total-pressure recovery with Mach number for  $\frac{m}{m_0} = 0.95$ . For  $\alpha = 0^\circ$  (fig. 11(a)) the total-pressure recoveries of the unswept and sweptback scoops were slightly higher and slightly lower, respectively, than that across a normal shock throughout the Mach number range. At  $\alpha = 10^\circ$  the

total-pressure recovery was obtained for the unswept scoop only at Mach numbers of 1.41 and 1.96; however, on the basis of the other variations of total-pressure recovery with Mach number it appears that above a Mach number of 1.5 the unswept scoop would have the higher recoveries. If a comparison of the total-pressure recoveries were made at a lower mass-flow ratio, the unswept scoop would show greater superiority than it does at  $\frac{m}{m_0} = 0.95$ .

#### CONCLUDING REMARKS

The present investigation was undertaken to study, principally at a Mach number of 1.41, the internal-flow characteristics of two forward underslung scoops with sector-shaped entrances. The sides of one scoop were unswept and the sides of the other were sweptback.

At a Mach number of 1.41, a mass-flow ratio of 0.95, and zero angle of attack each scoop provided a total-pressure recovery approximately equal to that across a normal shock at the free-stream Mach number; as the mass-flow ratio was decreased the total-pressure recovery of the unswept scoop remained nearly constant whereas that of the sweptback scoop decreased appreciably. The total-pressure recoveries of both scoops were higher at an angle of attack of  $10^\circ$  than at  $0^\circ$  throughout the mass-flow-ratio range.

From a total-pressure-recovery standpoint the unswept scoop appears to be a satisfactory configuration at a Mach number of 1.41. The lower total-pressure recovery of the sweptback scoop at the lower mass-flow ratios may not be a serious deficiency since the design mass-flow ratio at a Mach number of 1.41 will probably be high. Additional measurements of total-pressure recovery at transonic speeds and drag measurements are now needed to evaluate finally the worth of the scoop designs. Tests of a sweptforward sector-shaped scoop and a comparison of the performance of the sector-shaped scoops with other types of supersonic scoops on a fuselage with the nose rounded to meet current radar design requirements would also be of interest.

Langley Aeronautical Laboratory  
National Advisory Committee for Aeronautics  
Langley Field, Va.

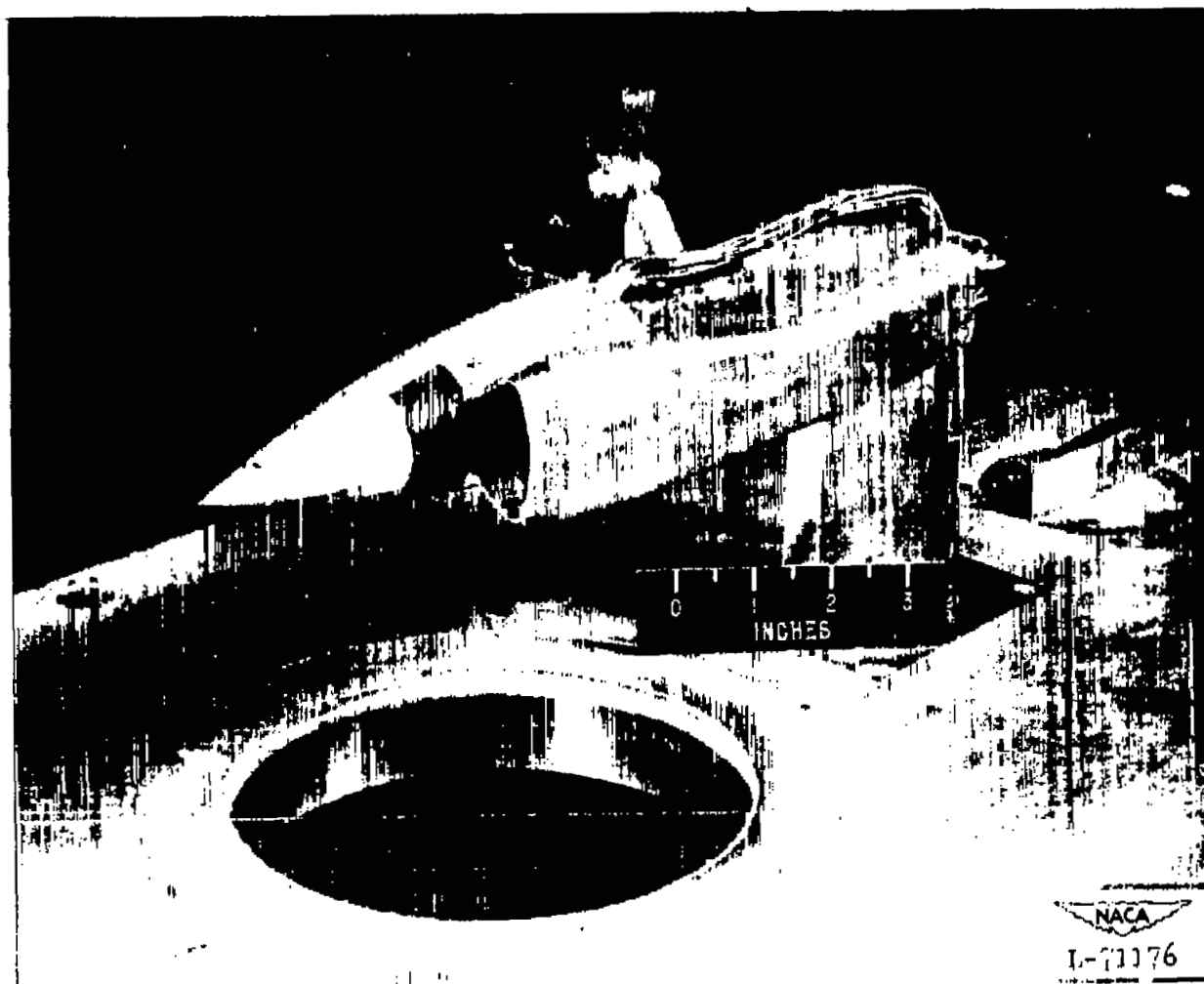
## REFERENCES

1. Wittliff, Charles E., and Byrne, Robert W.: Preliminary Investigation of a Supersonic Scoop Inlet Derived from a Conical-Spike Nose Inlet. NACA RM L51G11, 1951.
2. Merlet, Charles F., and Carter, Howard S.: Total-Pressure Recovery of a Circular Underslung Inlet with Three Different Nose Shapes at a Mach Number of 1.42. NACA RM L51K05, 1951.
3. May, Ellery B., Jr.: Investigation of the Effects of Leading-Edge Chord-Extensions on the Aerodynamic and Control Characteristics of Two Sweptback Wings at Mach Numbers of 1.41, 1.62, and 1.96. NACA RM L50L06a, 1951.



L-71394

Figure 1.- Scoop and forward part of fuselage of possible low-supersonic-speed airplane. Inlet area is 20 percent of maximum fuselage cross-sectional area.



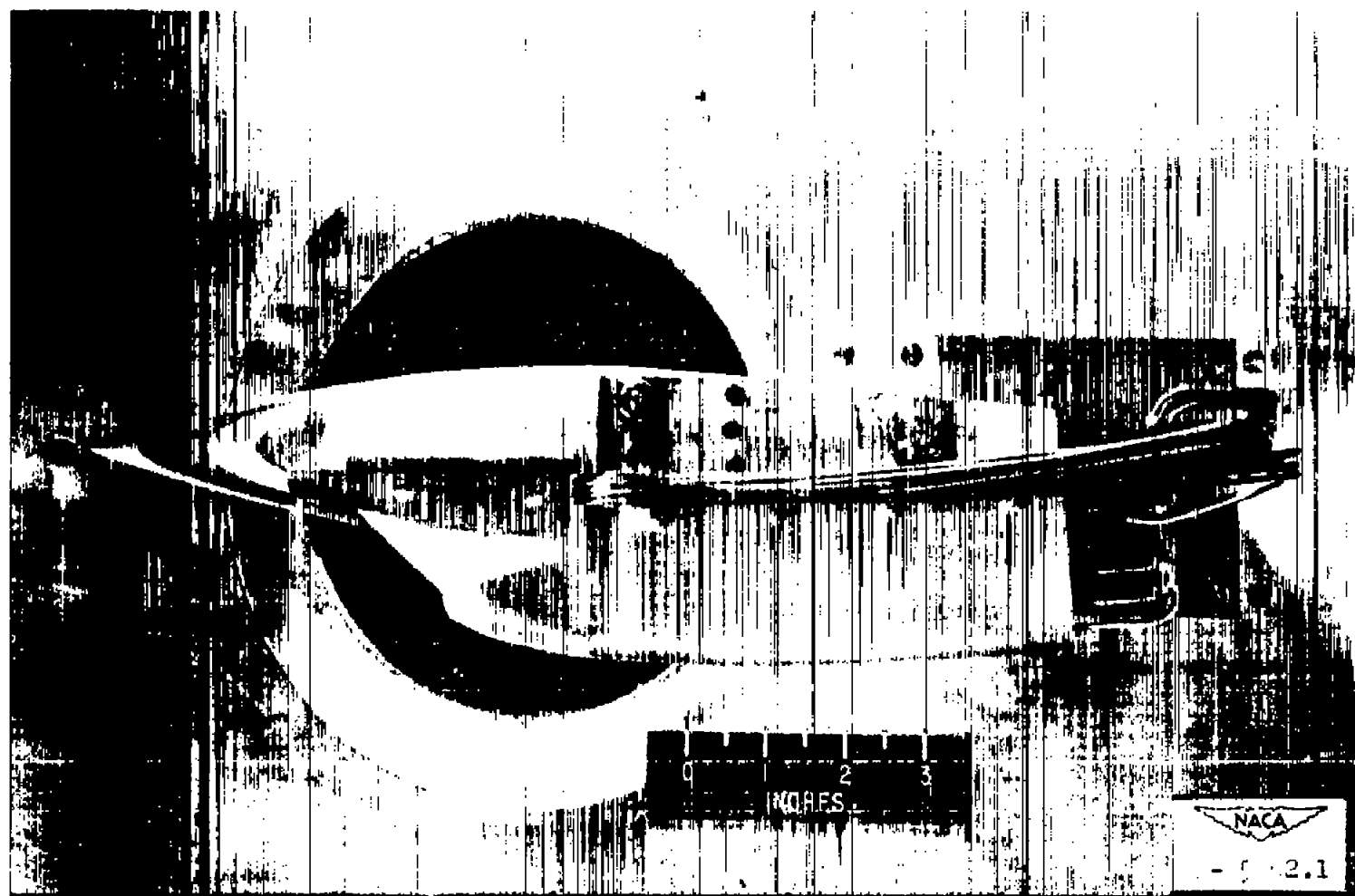
(a) Unswept scoop.

Figure 2.- Photographs of model mounted on tunnel strut.



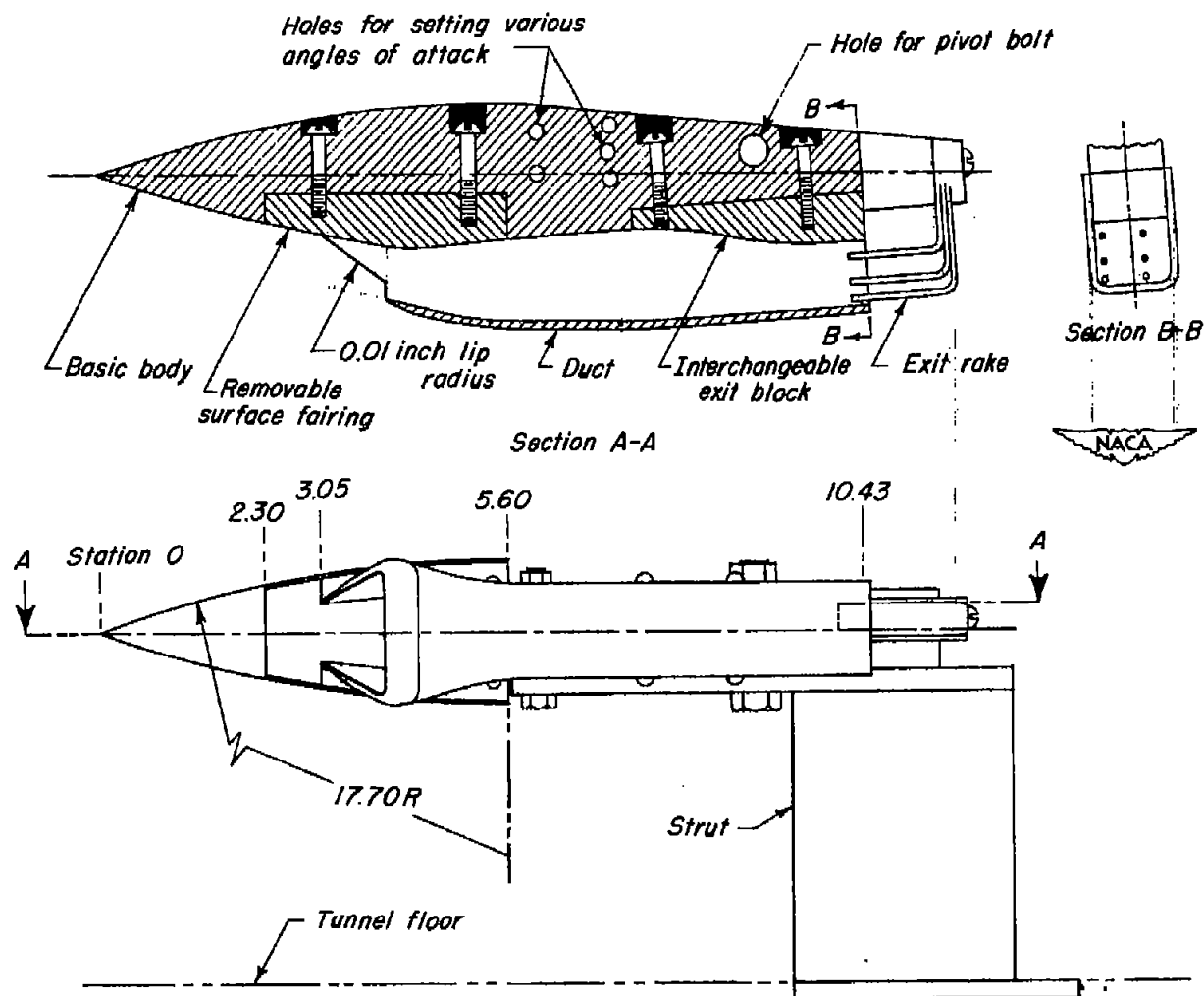
(b) Sweptback scoop, three-quarter front view.

Figure 2.- Continued.



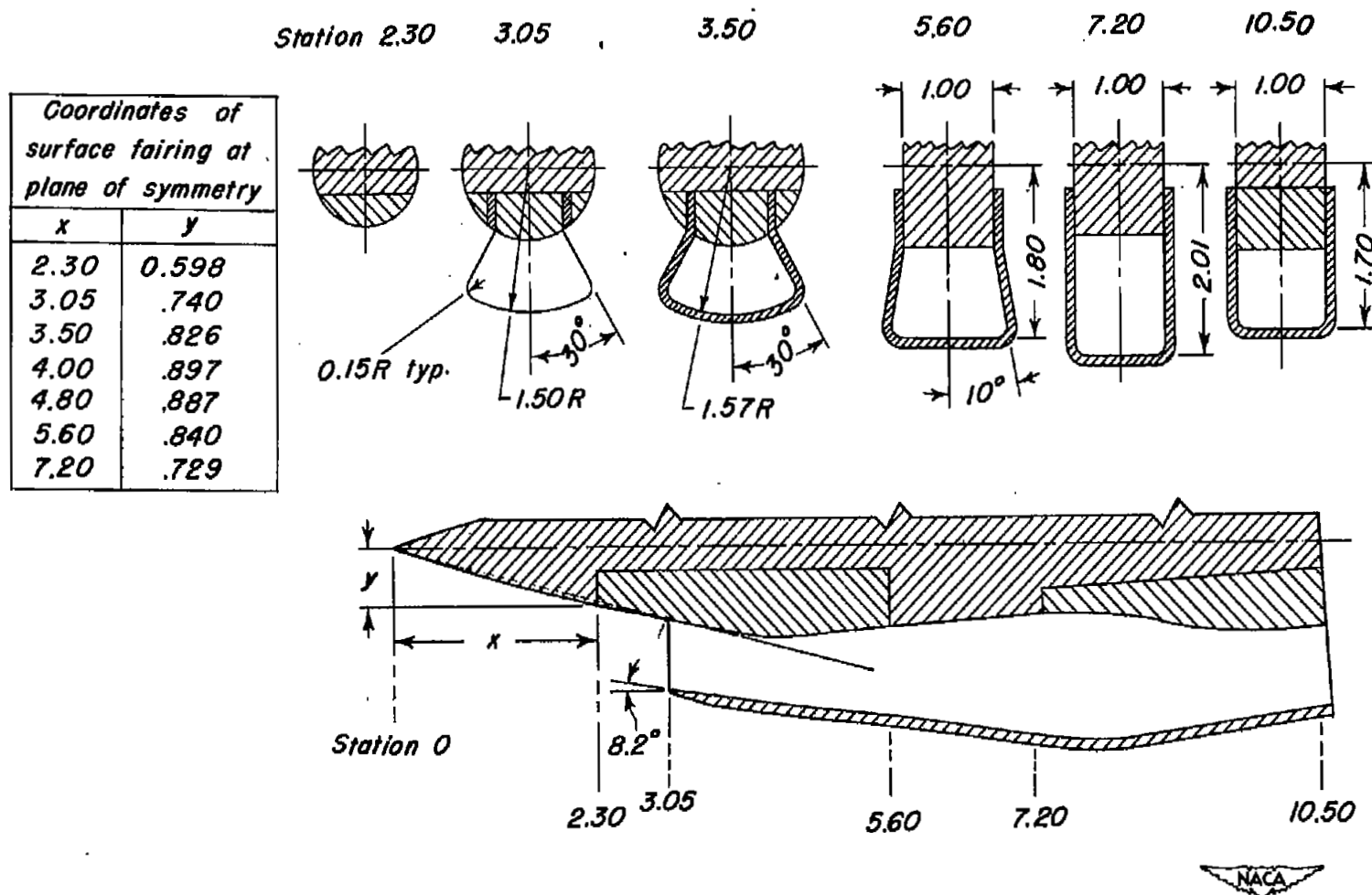
(c) Sweptback scoop, side view.

Figure 2.- Concluded.



(a) General arrangement.

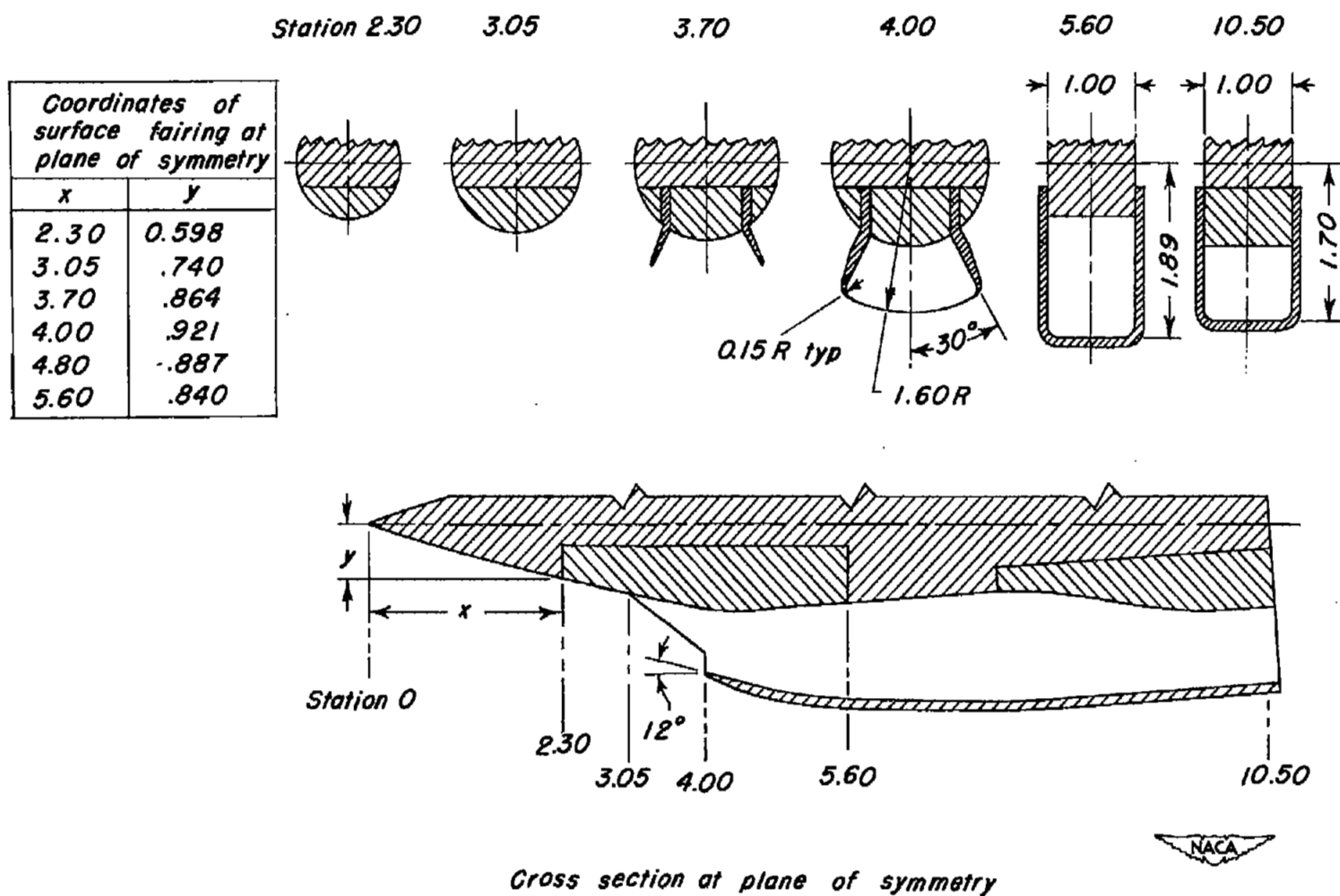
Figure 3.- Drawings of the model. (All dimensions are in inches.)



Cross section at plane of symmetry

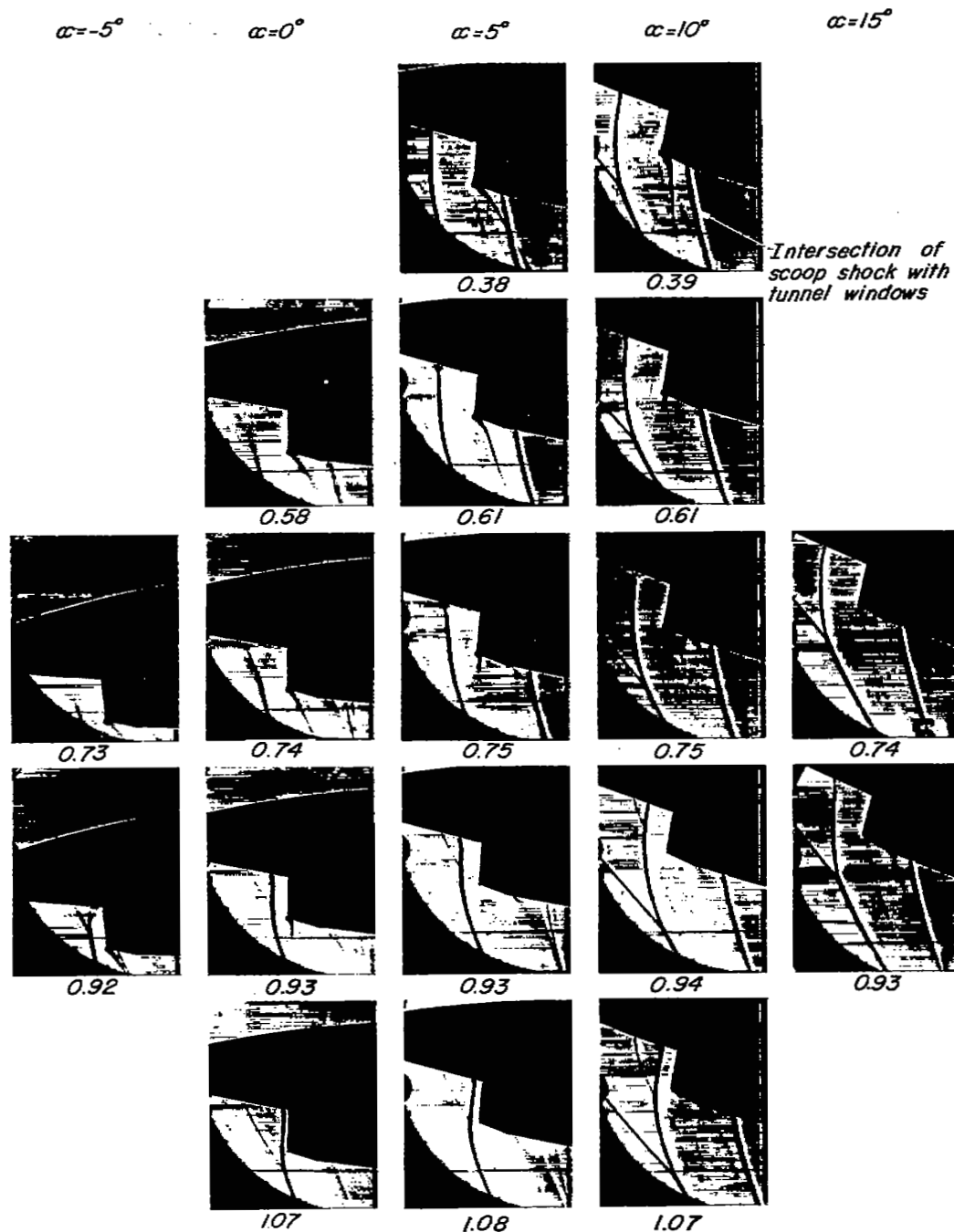
(b) Details of unswept scoop.

Figure 3.- Continued.



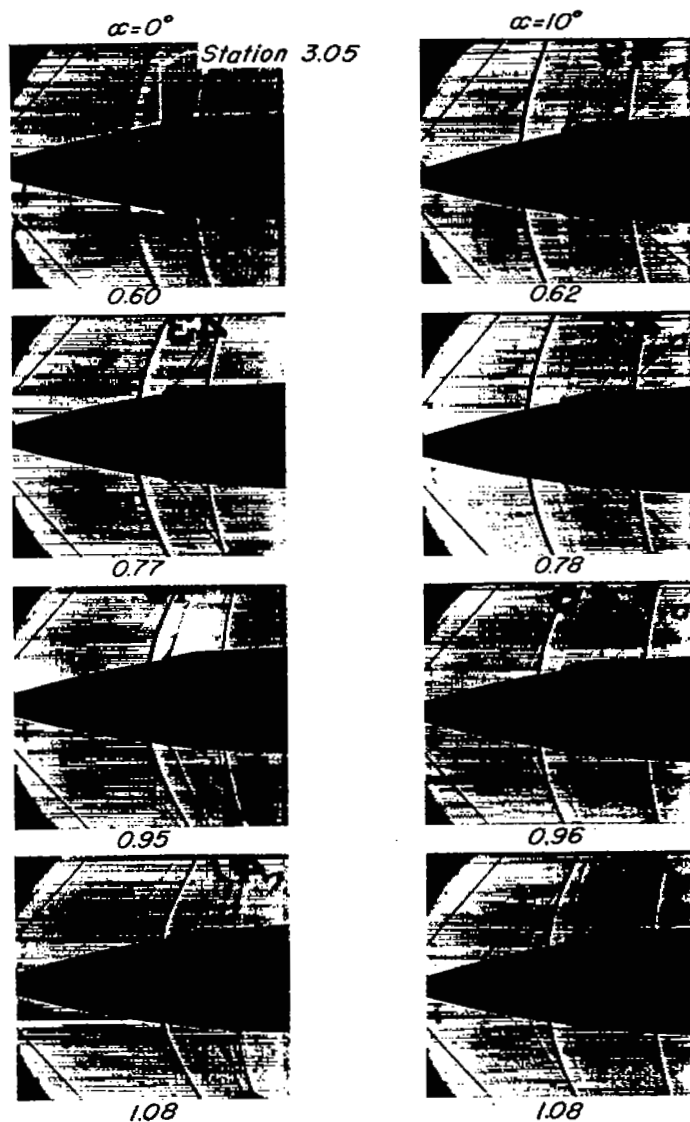
(c) Details of sweptback scoop.

Figure 3.- Concluded.



(a) Unswept scoop, side view,  $M_0 = 1.41$ . L-72708

Figure 4.- Shadowgraphs of the flow. (The angle of attack is indicated at the top of each column, and the mass-flow ratio under each shadowgraph.)

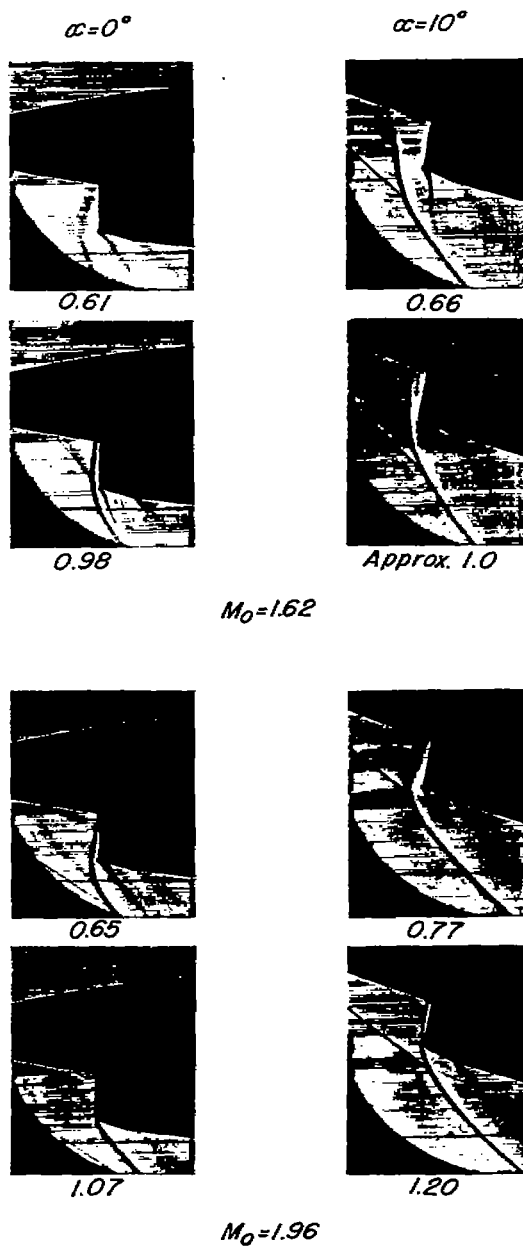


(b) Unswept scoop, top view,  $M_0 = 1.41$ .

Figure 4.- Continued.



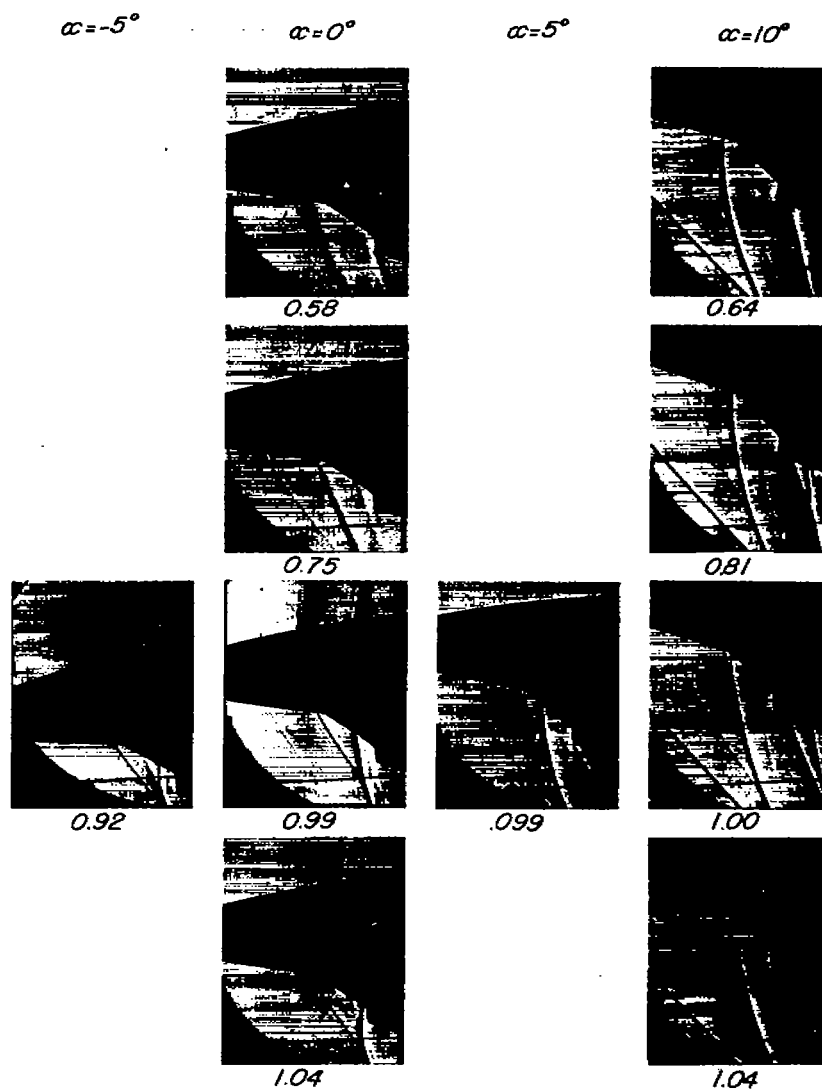
L-72709



(c) Unswept scoop, side view.

Figure 4.- Continued.

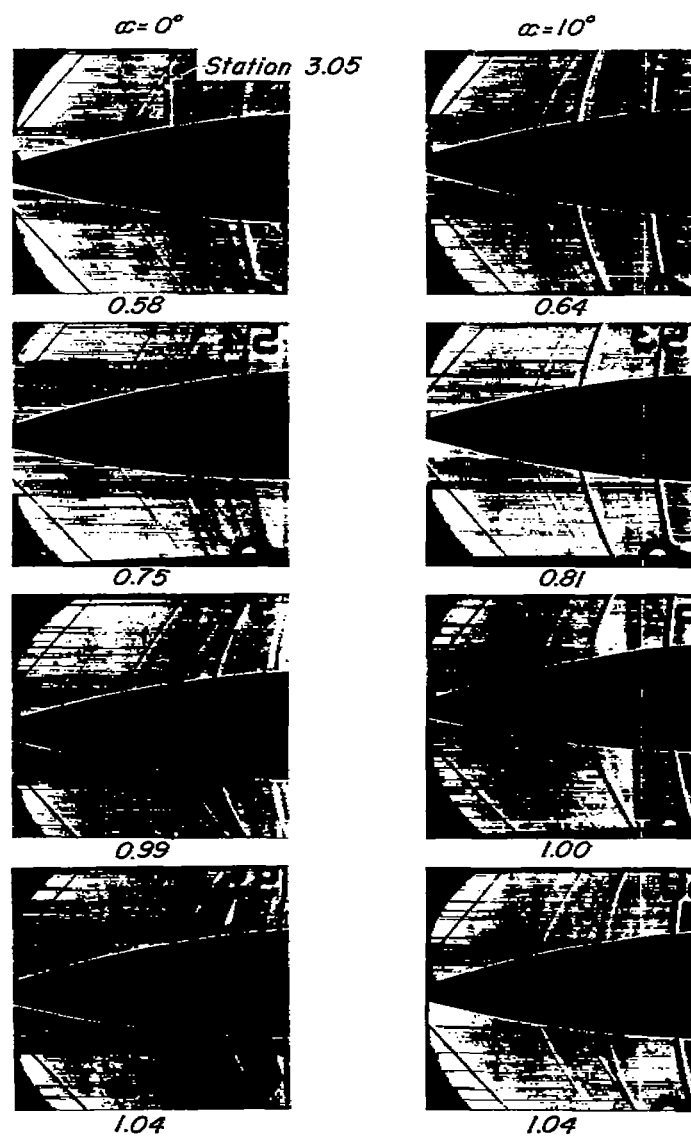
NACA  
L-72710



(d) Sweptback scoop, side view,  $M_0 = 1.41$ .

Figure 4.- Continued.

NACA  
L-72711

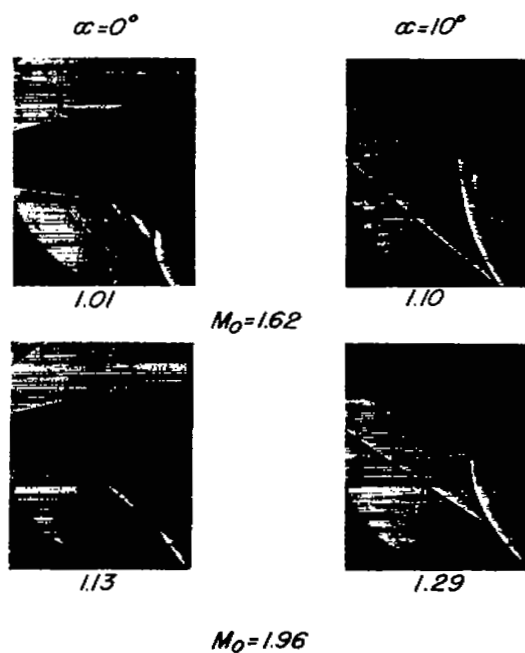


(e) Sweptback scoop, top view,  $M_0 = 1.41$ .

Figure 4.- Continued.



L-72712



(f) Sweptback scoop, side view.

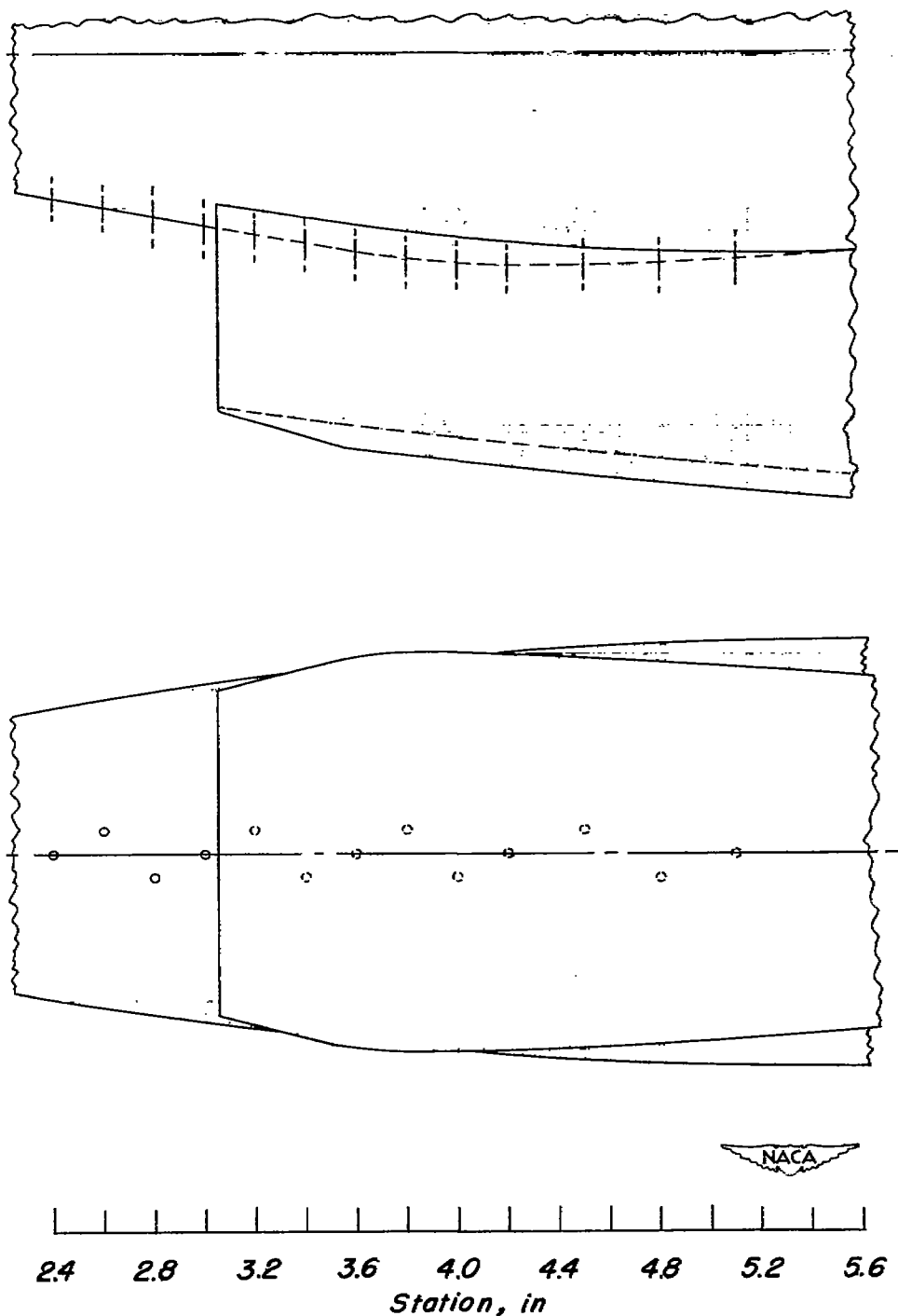
Figure 4.- Concluded.

NACA  
L-72713



Figure 5.- No-flow shadowgraphs.

NACA  
L-72714



(a) Pressure orifice locations.

Figure 6.- Surface-pressure distributions on fuselage; unswept scoop installed.

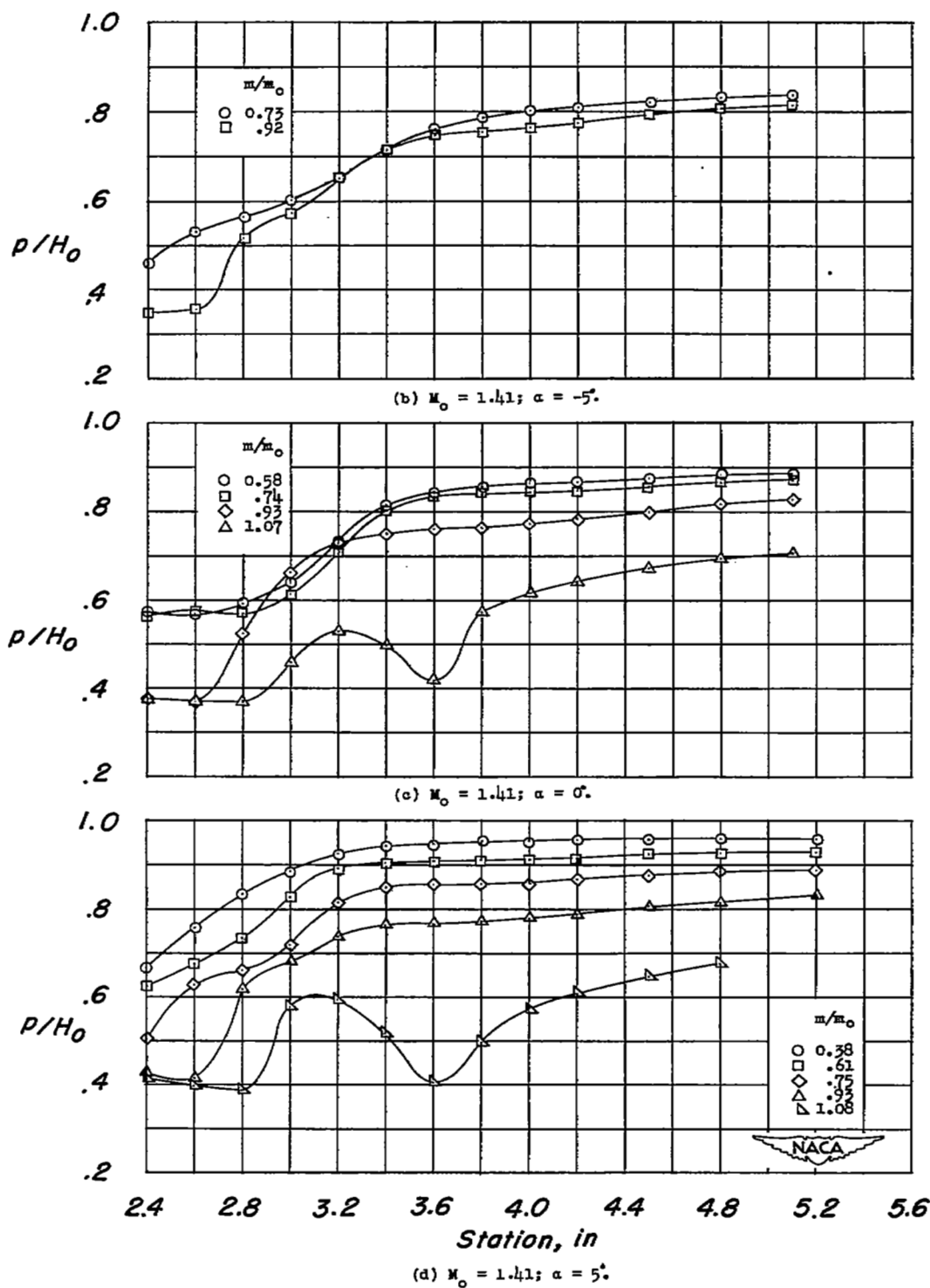


Figure 6.- Continued.

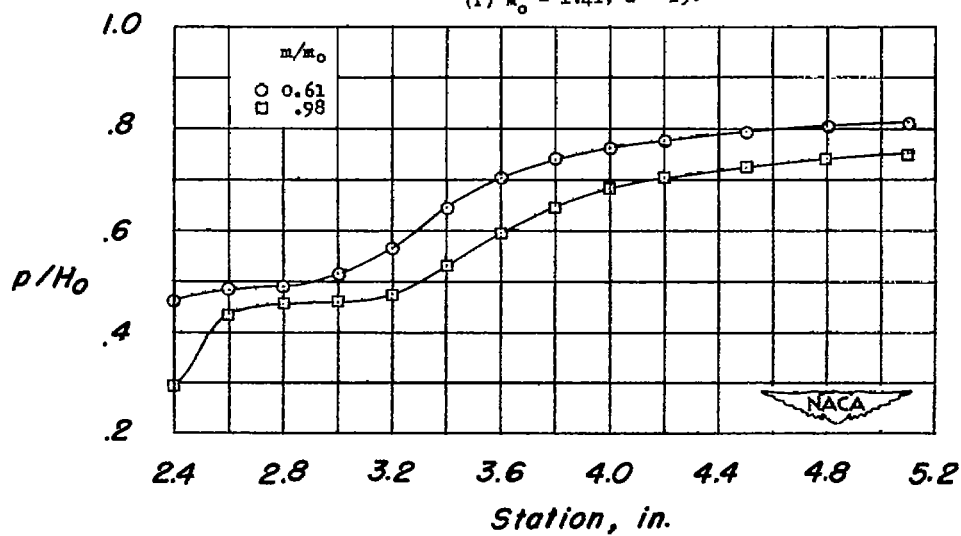
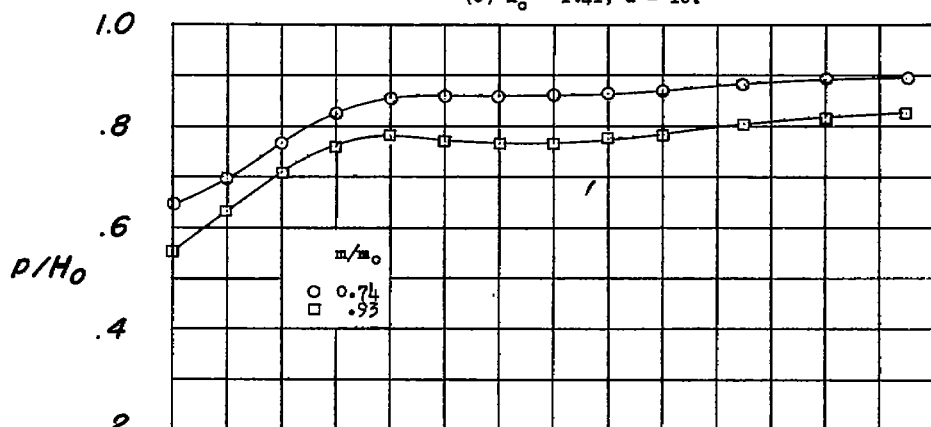
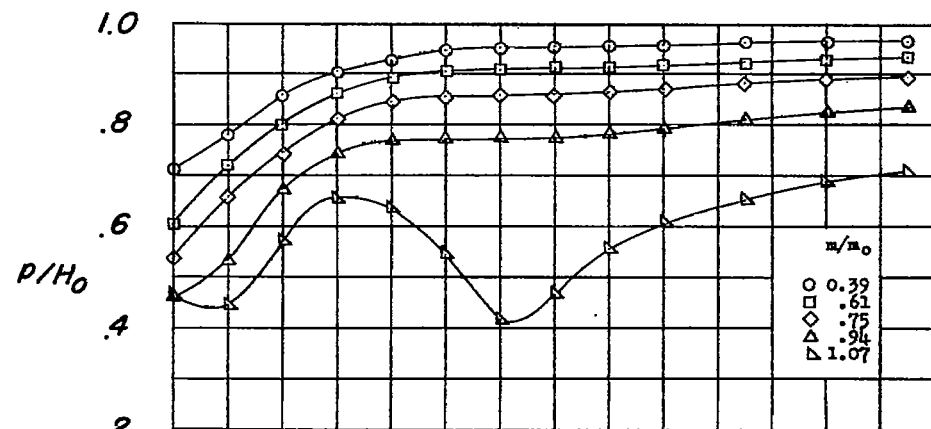


Figure 6.- Continued.

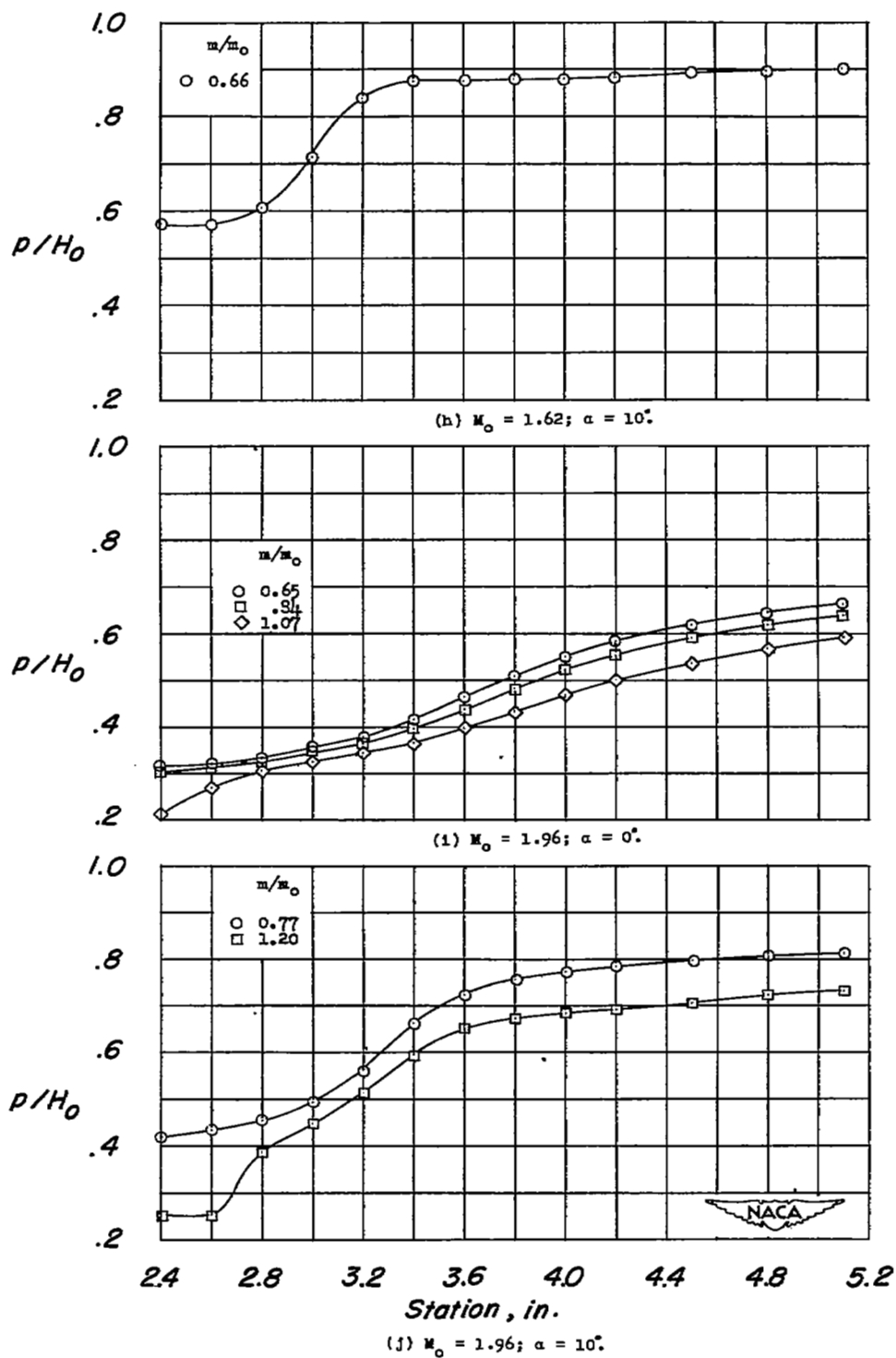


Figure 6.- Concluded.

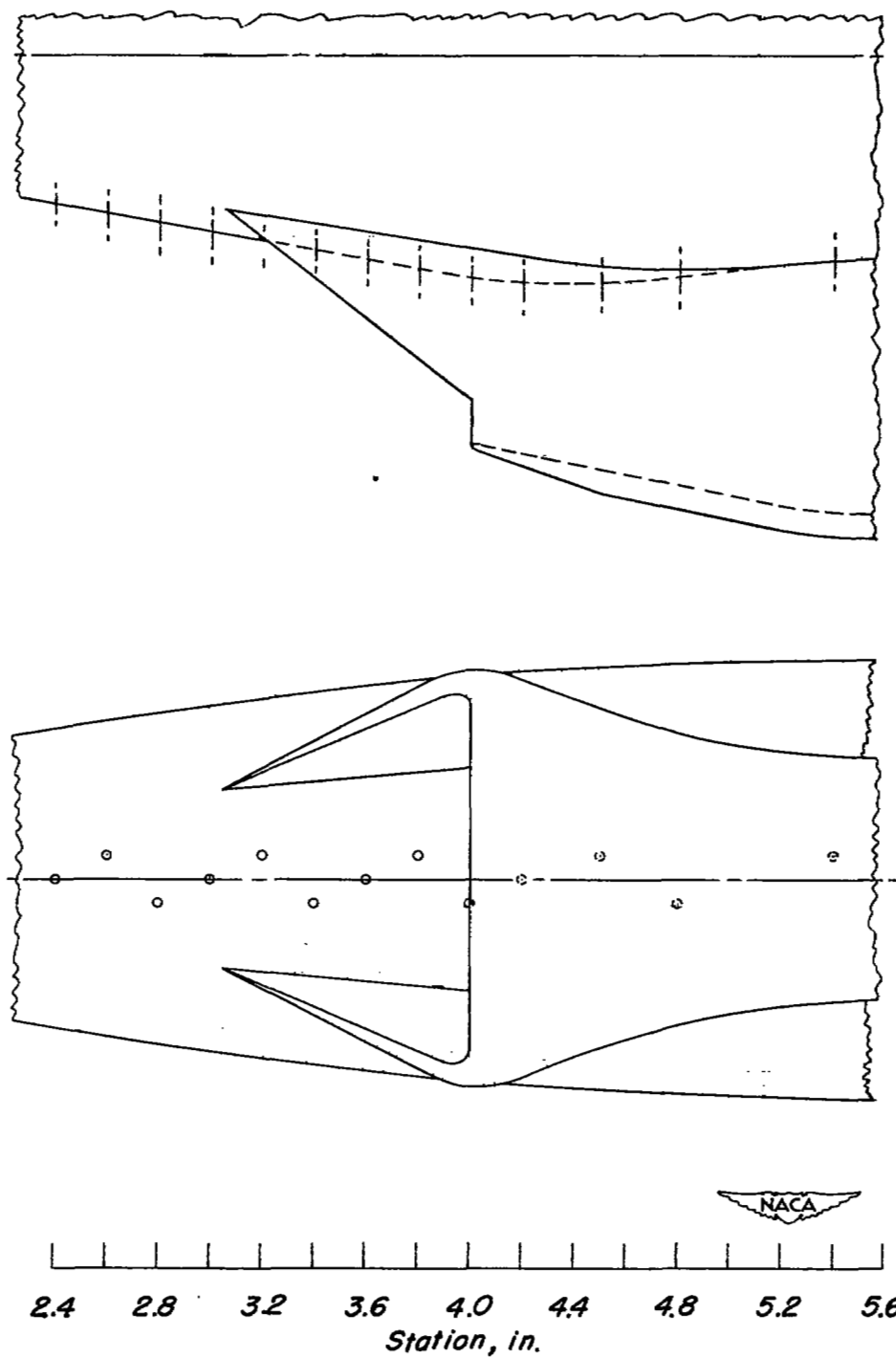


Figure 7.- Surface-pressure distribution on fuselage; sweptback scoop installed.

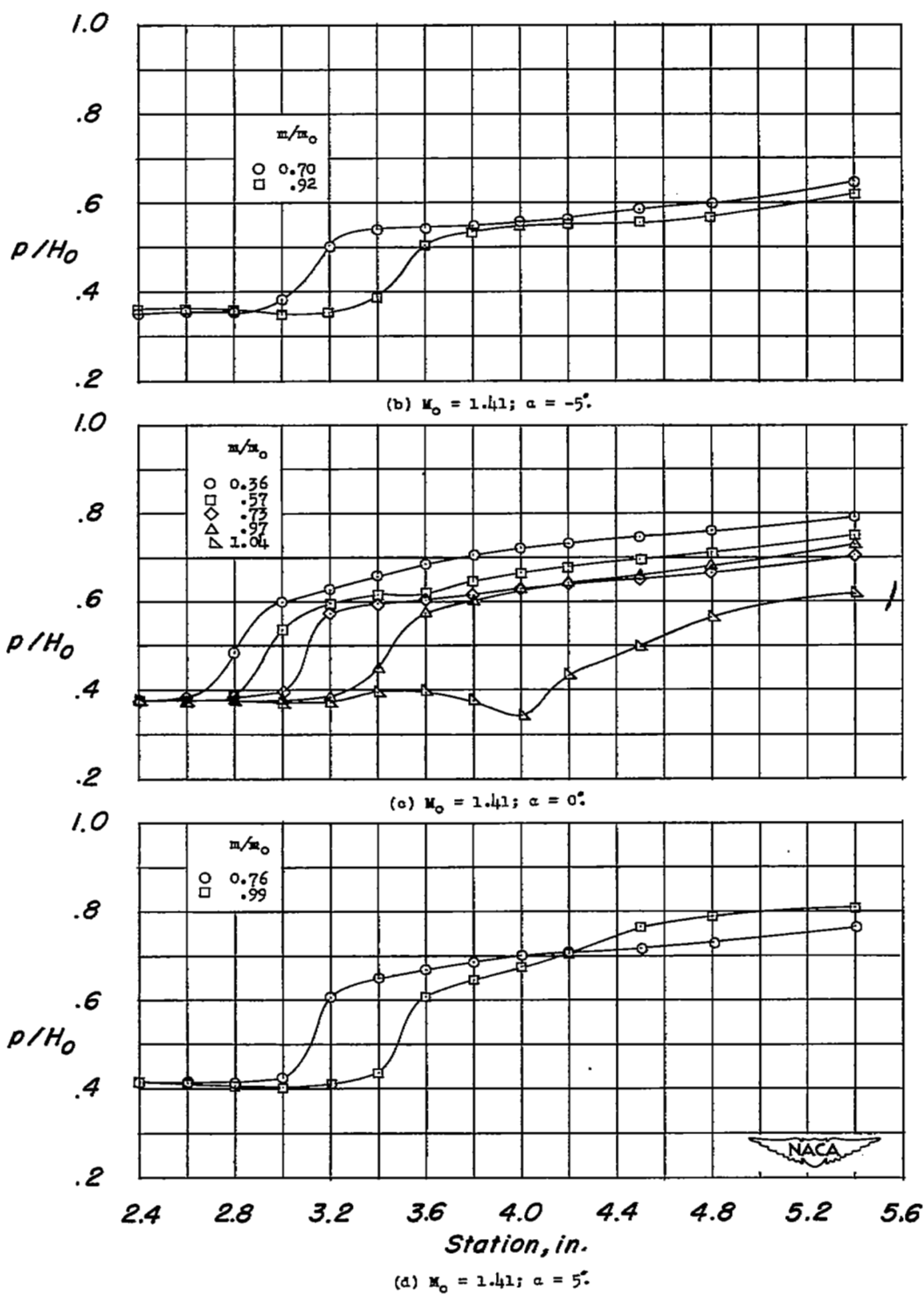


Figure 7.- Continued.

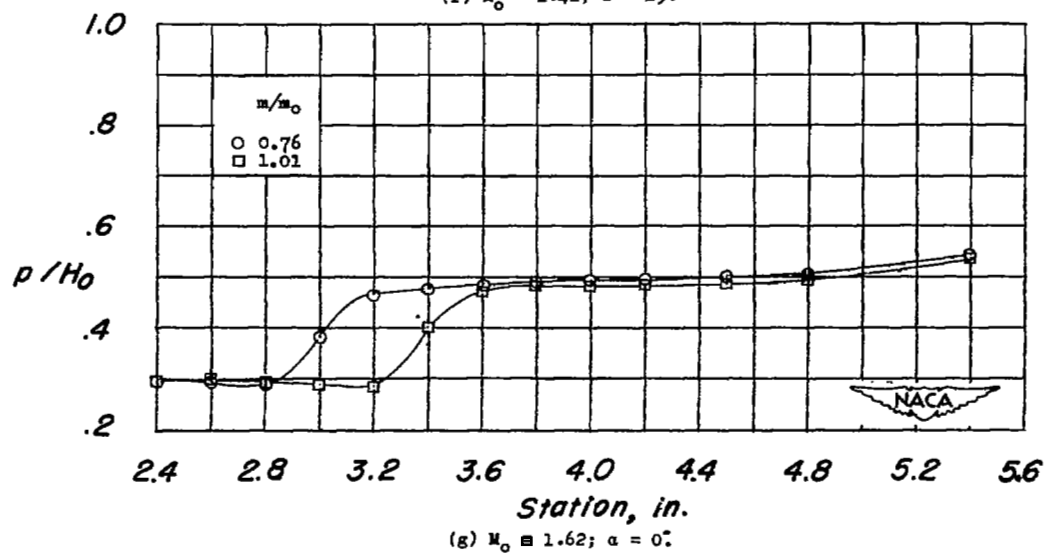
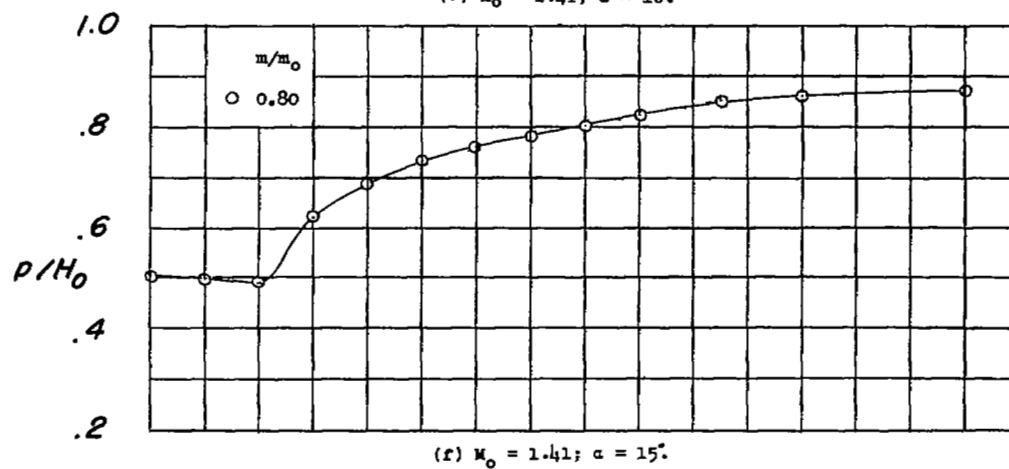
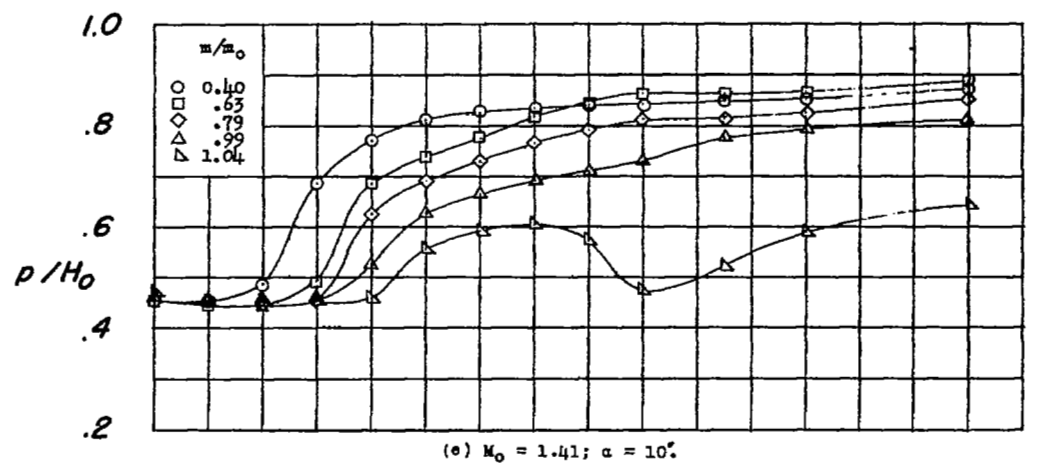


Figure 7.- Continued.

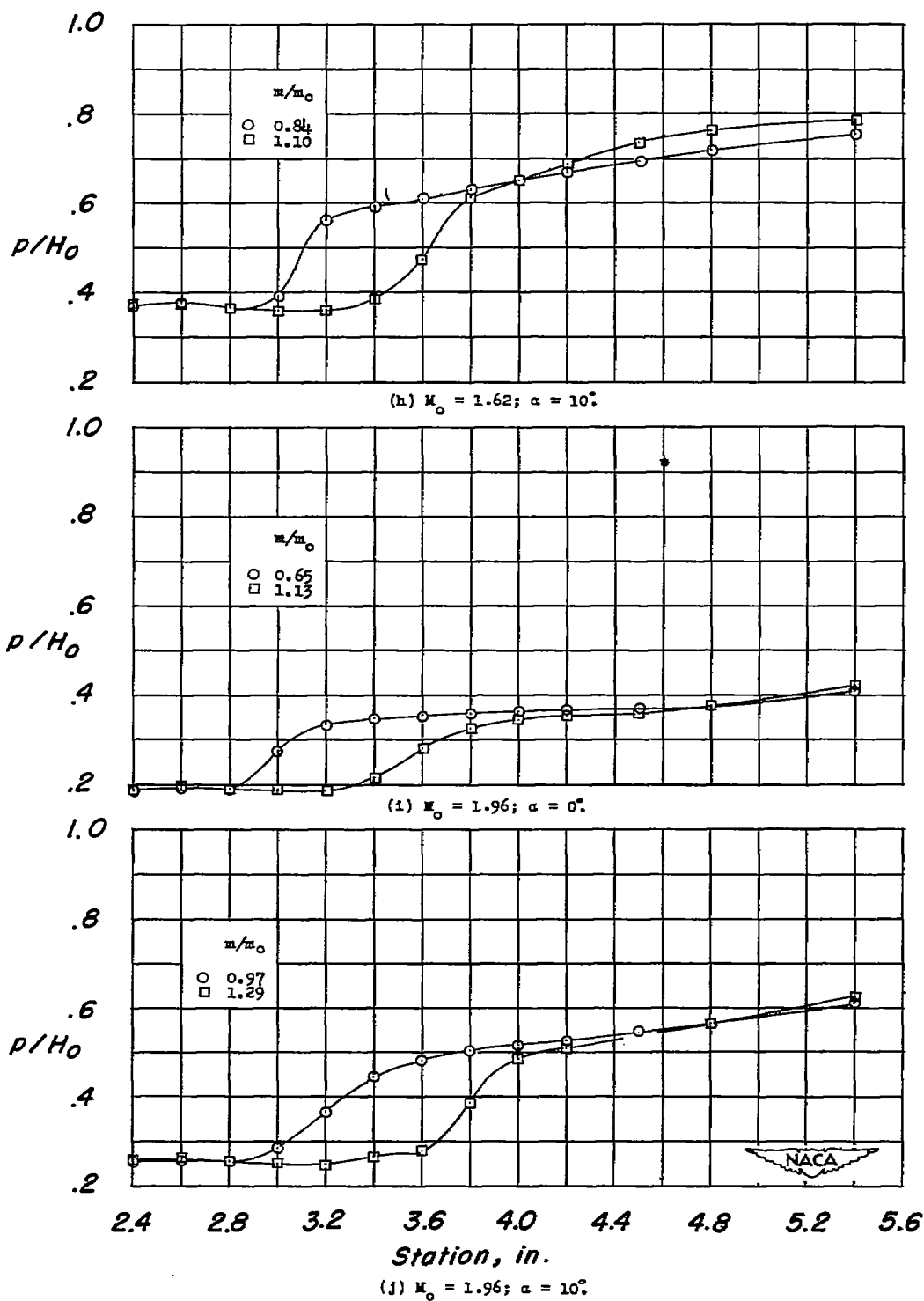


Figure 7.- Concluded.

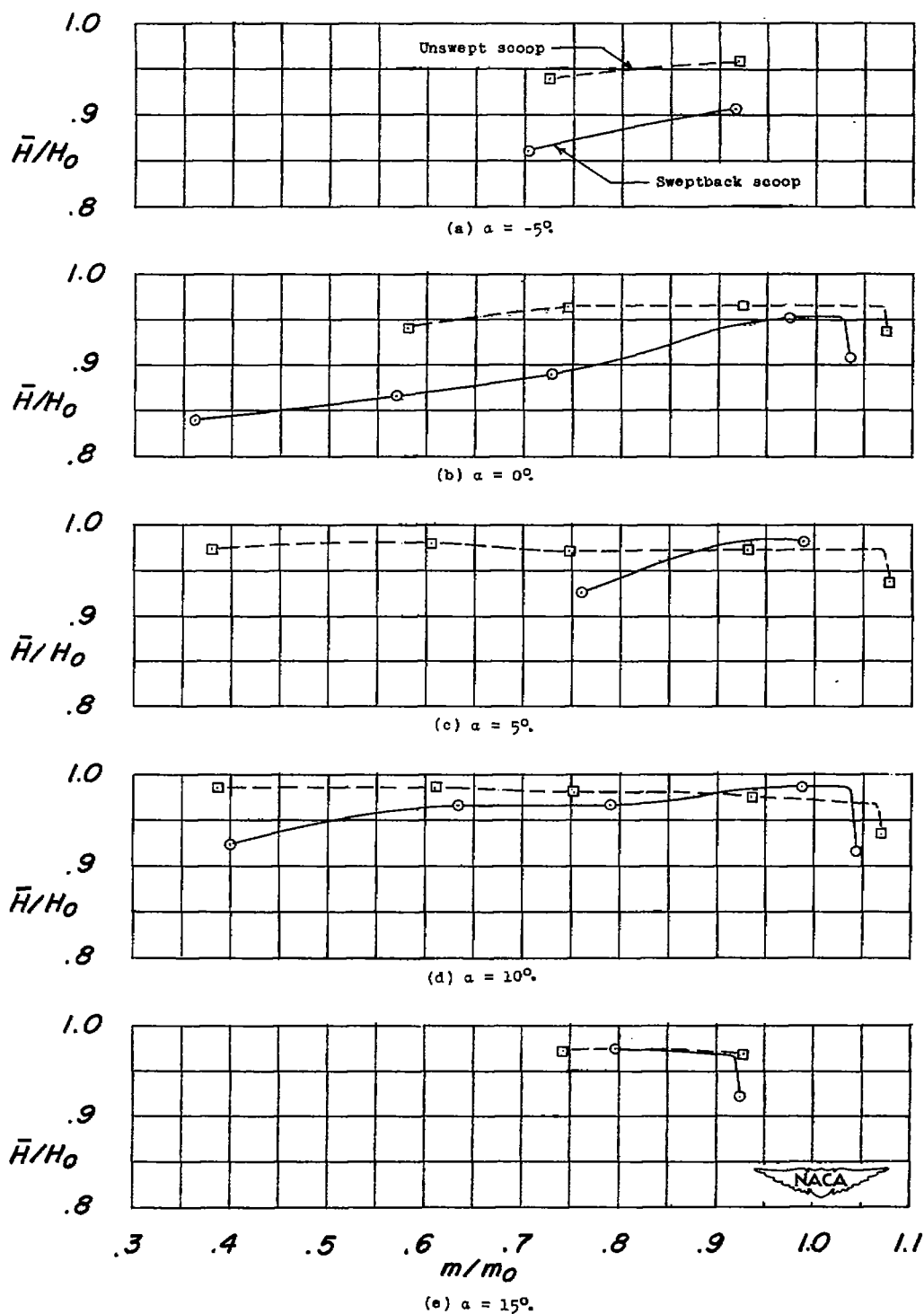


Figure 8.- Average total-pressure ratio as a function of mass-flow ratio;  $M_0 = 1.41$ .

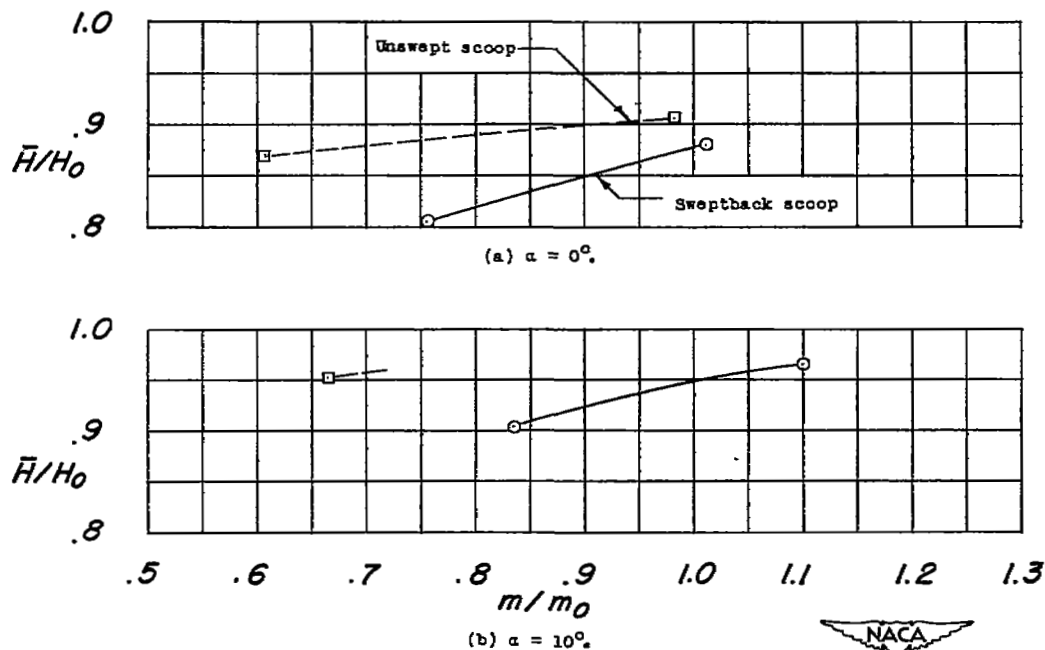


Figure 9.- Average total-pressure ratio as a function of mass-flow ratio;  $M_0 = 1.62$ .

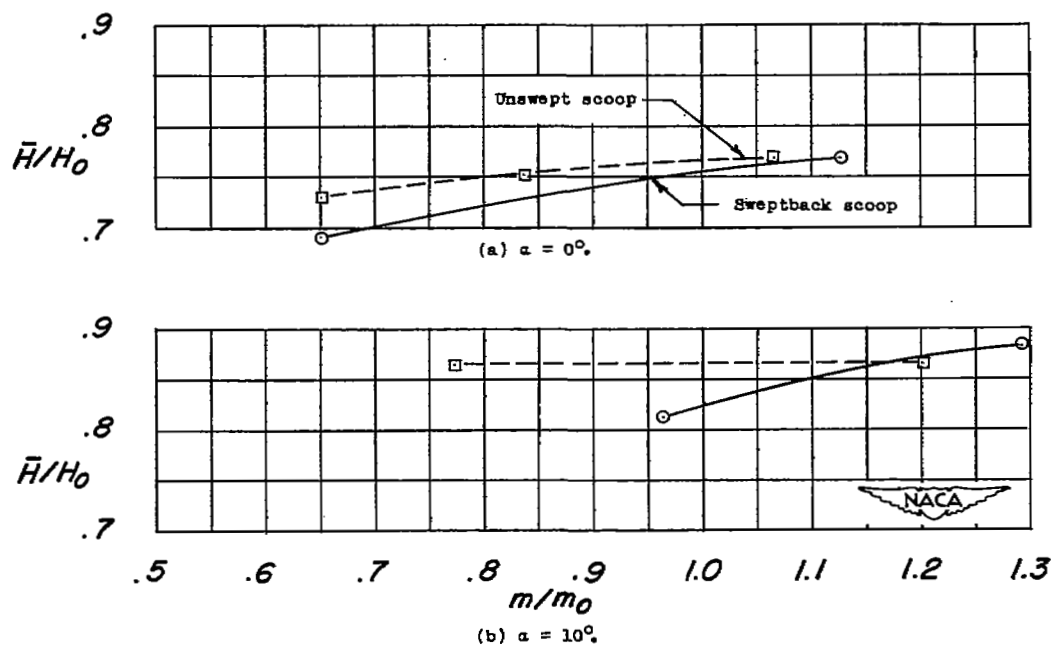


Figure 10.- Average total-pressure ratio as a function of mass-flow ratio;  $M_0 = 1.96$ .

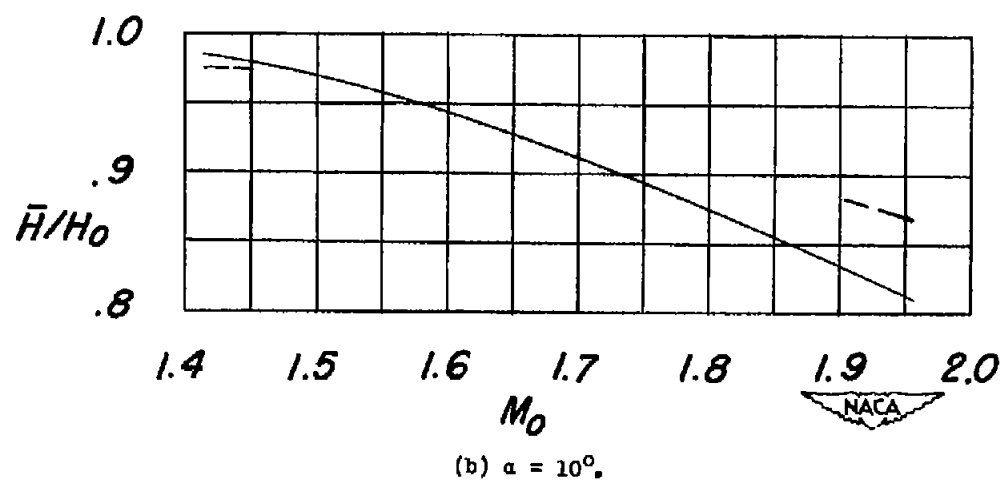
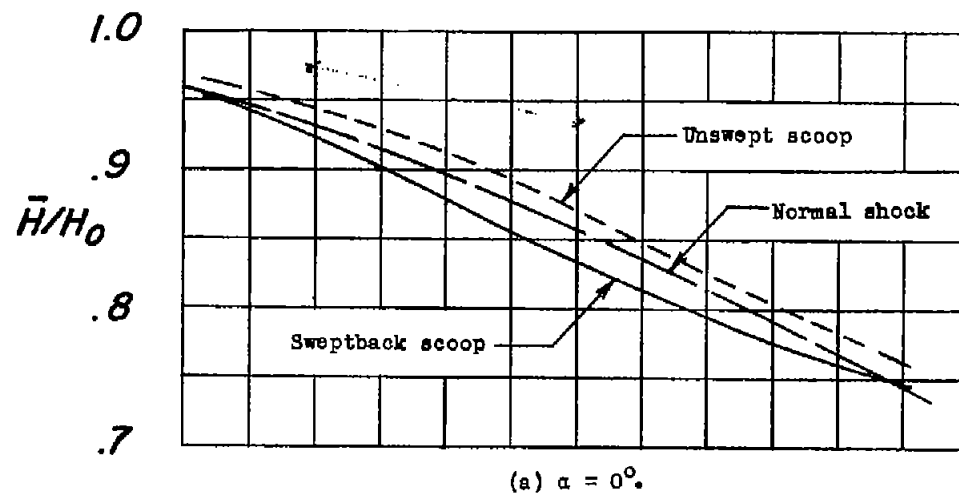
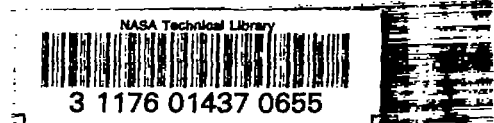


Figure 11.- Average total-pressure ratio as a function of Mach number;  
 $\frac{m}{m_0} = 0.95$ .

# SECURITY INFORMATION

[REDACTED]



[REDACTED]